Tăng cường khả năng bắt giữ khí SO_2 của $M_2(BDC)_2TED$ (M = Mg, V, Co, or Ni) bằng nghiên cứu tính toán

TÓM TẮT

Cùng với việc phát triển các nguồn năng lượng sạch bền vững thì bảo vệ môi trường là vấn đề hết sức cấp thiết vì không khí ngày càng ô nhiễm bởi các khí độc hại. Trong đó, khí SO_2 ảnh hưởng nghiêm trọng đến sức khỏe con người. Do đó, việc loại bỏ khí SO_2 làm sạch môi trường sống là vô cùng cấp bách. Đã có rất nhiều công nghệ khác nhau được đề xuất để giải quyết vấn đề này nhưng chưa thực sự hiệu quả. Sự nổi lên của vật liệu xốp có bề mặt riêng cực lớn và tính xốp siêu cao đã thu hút nghiên cứu bắt giữ khí SO_2. Trong đó, vật liệu khung hữu cơ kim loại rất được quan tâm trong lĩnh vực hấp phụ, tách lọc và một số ứng dụng tiềm năng khác. Trong nghiên cứu này, nhóm $M_2(BDC)_2TED$ (M = Mg, V, Co, Ni) được chọn để nghiên cứu bắt giữ SO_2 bằng phương pháp mô phỏng. Nghiên cứu được thực hiện tại nhiệt độ phòng 298 K và áp suất đến 2,5 bar. Kết quả chỉ ra thứ tự của kim loại làm tăng dần lượng khí SO_2 hấp phụ trong $M_2(BDC)_2(TED)$ là: Co < Ni < V < Mg. Tại 298K và 2.5 bar, lượng hấp phụ SO_2 trong Mg-MOF lớn nhất là khoảng 16 mmol/g và khoảng 13 – 14 mmol/g cho các M-MOF còn lại (M = V, Ni, Co). Nghiên cứu cũng làm sáng tỏ các yếu tố làm tăng cường hấp phụ SO_2 trong M-MOFs nói trên gồm nhiệt hấp phụ, diện tích bề mặt riêng (SSA) và thể tích rỗng (V_p). Đáng kể nhất là SSA và V_p của M-MOFs gần như làm tăng tuyến tính khả năng bắt giữ SO_2 ở nhiệt độ phòng và áp suất thấp.

Từ khóa: *$M_2(BDC)_2TED$, Monte Carlo chính tắc lớn, Bắt giữ SO_2, Diện tích bề mặt riêng, Thể tích rỗng*.

Computational study on enhancing SO_2 capture capacity of $M_2(BDC)_2TED$ (M = Mg, V, Co, or Ni)

ABSTRACT

Along with finding and developing sustainable clean energy sources, environmental protection is highly urgent because the air is increasingly polluted by more and more toxic gases. In particular, the presence of toxic gas SO_2 seriously affects human health. Therefore, removing toxic SO_2 gas to clean the living environment is extremely urgent. Many technologies have been suggested to solve this problem but have not been effective yet. In recent years, the emergence of porous materials with ultra-large specific surface areas and ultra-high porosity has attracted the attention of scientists in SO_2 capture. Among porous materials, metal-organic frameworks are intensely interested in adsorption, separation, and other potential applications. Here, we select the porous materials $M_2(BDC)_2TED$ (M = Mg, V, Co, Ni) to study the SO_2 capture using simulation approachs. The research was performed at room temperature 298 K and pressure under 2.5 bar. Our results show that the order of metals gradually increasing the SO_2 adsorption uptake in $M_2(BDC)_2(TED)$ is Co < Ni < V < Mg. Specifically, at 298K and 2.5 bar, the amount of SO_2 adsorption is about 16 mmol/g for Mg-MOF, and about 13 – 14 mol/g for the M-MOF (M = V, Ni, Co). The study also elucidated the influencing factors that enhance SO_2 adsorption in $M_2(BDC)_2TED$, including adsorption isosteric heat, specific surface area, and pore volume. Noticeably, the specific surface areas and pore volumes of M-MOFs almost linearly enhance the SO_2 capture capability at room temperature and low pressure.

Keywords: *$M_2(BDC)_2TED$, Grand canonical Monte Carlo, SO_2 capture, Specific surface area, Pore volume.*

1. INTRODUCTION

Sulfur dioxide (SO_2) is a colorless, non-flammable, and common pollutant in industrial production as well as daily life. Exposure to SO_2 may irritate the nose, throat, and eyes. Besides, SO_2 is a corrosive gas with high solubility (120 g/*l*) in water and can combine with water and air to form sulfuric acid, the main component of acid rain.[1,2,3] Despite the low SO_2 content in the air, it is classified as a toxic gas and one of the six most common environmental pollutants by the US Environmental Protection Organization.[4] Notably, significant amounts of sulfur oxides (SO_x), especially SO_2, are released into the environment after the combustion of petroleum-based fuels in internal combustion engines utilized in motorized vehicles.[3] Therefore, removing or reducing the quantities of SO_2 in the atmosphere is exceptionally urgent. Among many technologies, SO_2 capture based on the adsorption mechanism has been remarkable.[5] Metal-organic frameworks (MOFs) among porous materials are an exciting alternative for SO_2 capture due to outstanding structural properties such as ultrahigh surface area, high porosity, and controllable structural characteristics.[2,4] Therefore, SO_2 capture in nano-porous materials has attracted scientific interest. Many MOFs and other porous candidates have been studied and highly appreciated for SO_2 adsorption. Fu and co-workers showed that functionalized covalent triazine framework (CTF–CSU41) achieved the highest uptake of SO_2 with a maximum capacity of 6.7 mmol/g (*i.e.*, 42.9 wt%) at (298 K, 0.15 bar).[3,6] For MOFs, MOF-177 exhibited the highest SO_2 uptake with 25.7 mmol/g at (293 K, 1 bar). Some other MOFs also showed high SO_2 capture capacity, ranging from 4,8 to 17,3 mmol/g.[3] Besides many other MOFs, $M_2(BDC)_2(TED)$ or $M(BDC)(TED)_{0.5}$ materials have been attractive for applications in capturing toxic gases (CO_2, SO_2, CH_4, NH_3, H_2S, NO_x, …).[4] In this research, we use simulations to find optimum $M_2(BDC)_2(TED)$ MOFs for SO_2 capture, where M is magnesium (Mg), vanadium (V), cobalt (Co) or nickel (Ni); BDC = 1,4-Benzenedicarboxylate; TED = Triethylen-diamine or DABCO: 1.4-Diazabicyclo[2.2.2]octane.[7]

2. COMPUTATIONAL PHYSICS

The research approach combines density functional theory (DFT) calculations and grand canonical Monte Carlo (GCMC) simulations. Firstly, we used DFT calculations to optimize the geometries of $M_2(BDC)_2(TED)$ MOFs, namely M-MOFs. Secondly, GCMC simulations were used to obtain the isotherms and isosteric heat of SO_2 adsorption as well as calculate the structural characteristics of the M-MOFs.

To optimize the unit cell and extract partial atomic charges of the M-MOFs, we utilized the Vienna ab initio simulation package (VASP)[8,9] for the van der Waals dispersion-corrected density functional

theory (vdW-DF).[10,11] The plane-wave basis set with the cut-off energy of 700 eV for the plane-wave basis set.[12,13] We performed the surface Brillouin-zone integrations using the Monkhorst and Pack *k*-point sampling technique with the 3×3×3 mesh grid and the Gamma point at the center.[14] The Methfessel-Paxton smearing of order 1 was used for the ions and geometry relaxation, and atomic charge calculation with the smearing width sigma of 0.1 eV.[15]

GCMC simulations using the RASPA code were selected to study the gravimetric uptakes of SO_2 in the M-MOFs.[16] These simulations were performed in constant volume, temperature, and chemical potential at room temperature (298 K) and pressures up to 2.5 bar. The number of 300,000 MC steps were simulated for the random insertion, deletion, translation, and rotation of SO_2 molecules in the simulation box, repeated 3×3×3 times of the primary unit cell along the *a*, *b*, and *c* lengths.

The interactions between atoms of SO_2 gas and the MOFs were described by (*i*) the Coulombic or electrostatic interactions with its cut-off radius of 13 Å, and (*ii*) the van der Waals interactions with the simple Lennard-Jones (LJ) model with the LJ cut-off radius of 20 Å.[17,18] The cut-off radius and other parameters were carefully checked before performing the GCMC simulation. The partial charges of atoms of the M-MOFs were extracted from the density-derived electrostatic and chemical (DDEC6) atomic charges method, listed in Table 1, with the symbols for the atoms shown in Figure 1.[19–22] The qualities of the LJ potential well depth and diameter were determined by the Lorentz−Berthelot combining rules, one of the most common types of mixing rules for unlike atoms.[23,24] The parameters for σ_i and ε_i (i refers to the atoms like Fe, H, C, O in the M-MOFs or S, O in SO_2) were selected from the generic force fields for MOFs in the RASPA software package.[16,25]

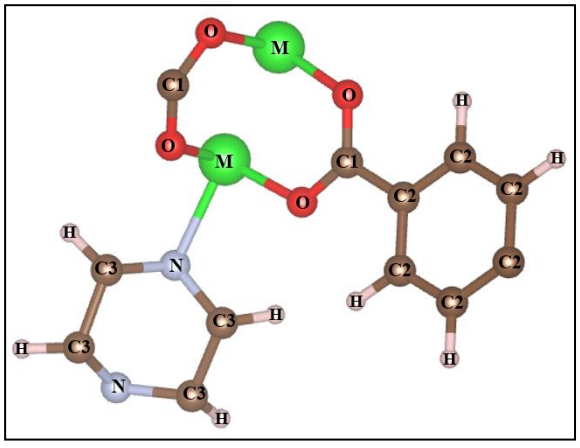

Figure 1. The symbol for atomic types with different charges of M-MOFs.

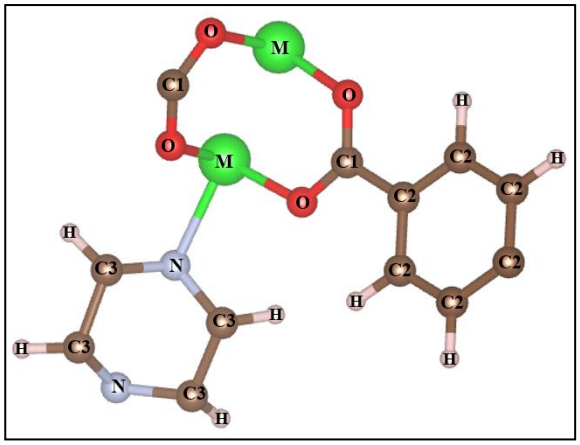

Figure 1. The symbol for atomic types with different charges of M-MOFs.

Table 1. The LJ (ε, σ) and charge parameters (q) for atomic types of M-MOFs and SO_2.

M-MOFs	Atomic types	LJ parameters		*q* (*e*)
		ε/k_B (K)	σ (Å)	
M = Mg	C1	47.856	3.472	0.739
	C2			-0.073
	C3			0.011
	H	7.648	2.846	0.088
	N	38.949	3.262	-0.362
	O	48.158	3.033	-0.721
	Mg	**55.857**	**2.691**	**1.385**
M = V	C1	47.856	3.472	0.627
	C2			-0.073
	C3			-0.012
	H	7.648	2.846	0.076
	N	38.949	3.262	-0.174
	O	48.158	3.033	-0.574
	V	**8,051**	**2,801**	**0.926**
M = Co	C1	47.856	3.472	0.613
	C2			-0.071
	C3			-0.025
	H	7.648	2.846	0.076
	N	38.949	3.262	-0.099
	O	48.158	3.033	-0.491
	Co	**7.045**	**2.558**	**0.573**
M = Ni	C1	47.856	3.472	0.636
	C2			-0.071
	C3			-0.025
	H	7.648	2.846	0.079
	N	38.949	3.262	-0.118
	O	48.158	3.033	-0.539
	Ni	**7.548**	**2.524**	**0,660**
SO_2[25,26]	O	58.725	3.198	-0.201
	S	189.353	3.410	0.402

3. RESULTS AND DISCUSSION

3.1. Optimization of the unit cell of $M_2(BDC)_2(TED)$

First, we constructed a unit cell based on experimental and computational works for $Ni_2(BDC)_2(TED)$ (BDC = Benzene dicarboxylate, and TED = Triethylenediamine) (Figure 2).[4,27] We optimized all ions and the size of the unit cells. Then, we replaced Ni with other bivalent metals such as Mg, V, and Co, which often appear in MOFs and greatly influence gas adsorption. The results obtained for the unit cells are listed in Table 2 and compared with the experimental data for M = Ni,[27] showing that these optimal results show reliability with 1.61%, 1.57%, and 4.81% for *a* (or *b*), *c* lengths, and the cell volume. The unit cell volume ($V_{M\text{-}MOF}$) of the M-MOFs also does not change much, and they are in slightly increasing order: $V_{Co\text{-}MOF} < V_{V\text{-}MOF} \approx V_{Ni\text{-}MOF} < V_{Mg\text{-}MOF}$.

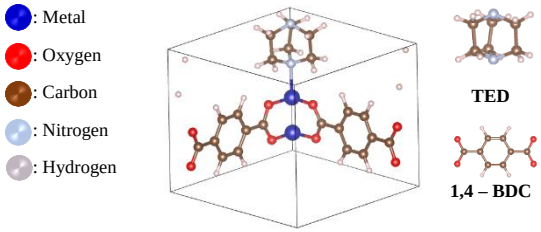

Figure 2. A primary unit cell of M-MOFs (M = Mg, V, Co or Ni).

Table 2. The optimized parameters of the unit cell of the $M_2(BDC)_2TED$ structures, compared with other works.

$M_2(BDC)_2TED$	Lattice constant (Å)		Volume of unit cell (Å^3)
	a = *b*	*c*	
M = Mg	10.98	9.39	1130
M = V	10.96	9.37	1125
M = Co	10.90	9.31	1113
M = Ni	10.97	9.38	1128
M = Ni (exp. data)[28]	11.15	9.53	1185
Error compared exp. data (%)	1.61	1.57	4.81

3.2. The SO_2 capture capability of $M_2(BDC)_2TED$ MOFs

The SO_2 adsorption isotherms are shown in Figure 3 for both excess and absolute uptakes at pressures up to 2.5 bar. The results show these two uptakes are nearly similar for SO_2 on the M-MOFs (M = Mg, V, Co, or Ni) at low pressure under 2.5 bar. The adsorption uptakes for all metals are listed in Table 3. Our data are also compared to other ones. Compared to MOF-177, the best SO_2 capture to date, M-MOFs strongly adsorb SO_2 at low pressure below 0.5 bar.[1] On the contrary, above 0.5 bar, MOF-177 shows an outstanding uptake compared to our M-MOFs and other MOFs.[1]

The adsorption tendency in Mg-MOF is more substantial than in Ni-MOF, which is consistent with the experimental data of Kui Tan et al. at the same temperature and pressure conditions (0.11 bar, 298 K),[27] and and V. B. López-Cervantes et al (Table 3).[29,30] In this work, we study the adsorption capacity of M-MOFs for SO_2 up to a pressure of 2.5 bar because researching at high pressures is unnecessary, and the results achieved only change a little.[17] The results show that Mg-MOF has the strongest adsorption of SO_2, followed by V-MOF, Ni-MOF, and Co-MOF. Here, Mg-MOF adsorbs superiorly compared to the remaining M-MOFs (M = V, Ni, Co). At 2.5 bar and 298 K, the the best uptakes reach for Mg-MOF with $n_{exc} = 15.82$ mmol/g, $n_{abs} = 15.92$ mmol/g, followed by V-MOF ($n_{exc} = 13.77$ mmol/g, $n_{abs} = 13.85$ mmol/g), Ni-MOF ($n_{exc} = 13.46$ mmol/g, $n_{abs} = 13.54$ mmol/g), and Co-MOF ($n_{exc} = 13.00$ mmol/g, $n_{abs} = 13.08$ mmol/g).

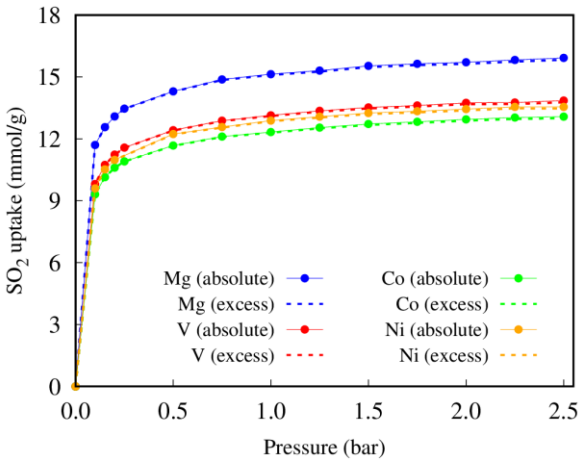

Figure 3. Absolute and excess isotherms of SO_2 on $M_2(BDC)_2(TED)$ at 298 K, where dashed lines and solid lines refer to absolute and excess uptakes.

Table 3. Absolute and excess SO_2 uptakes on $M_2(BDC)_2(TED)$ at 298 K and the pressures under 2.5 bar.

M-MOFs	SO_2 uptakes at 298 K, (mmol/g)		
	0.1 bar	1 bar	2.5 bar
M = Mg	11.69	15.13	15.92
M = V	9.80	13.13	13.85
M = Co	9.31	12.32	13.07
M = Ni	9.59	12.88	13.54
M = Ni[17]			13.6 (50 bar)
M = Mg[27]	6.44 (0.11 bar)	8.60 (1.02 bar)	
M = Ni[27]	4.54 (0.11 bar)	9.97 (1.13 bar)	
Mg(II)-MOF[29]		19.5	
Ni(II)-MOF[30]		12.5	
MOF-177[1,29]	1.3	25.7 (maximum, 293 K, 0.97 bar)	-

3.3. Effect of structural characteristics and isosteric heat on the SO_2 adsorption of $M_2(BDC)_2(TED)$

To explain the reason Mg increases the ability to capture SO_2 based on the adsorption mechanism compared to other metals, we analyze the factors that have a substantial impact on the gas adsorption of MOFs, which are the structural characteristics (specific surface area and pore volume) and adsorption isosteric heat.

Isosteric heat of adsorption, Q_{st}, is an essential factor required to describe the thermal performance of adsorptive systems.[31] The Q_{st} of SO_2 for the M-MOF series calculated in low pressures under 1.0 kPa are presented in Figure 4. The results show that Q_{st} tends to increase as pressure increases. However, the values change little in the low-pressure region. At higher pressures, the Q_{st} value of SO_2 for M-MOFs is most significant for Mg-MOF, rising from 42.03 kJ/mol to 47.97 kJ/mol. Meanwhile, other M-MOFs increase slightly with pressure. Specifically, uptakes of SO_2 in V-MOF: 40.61 – 44.73 kJ/mol, Co-MOF: 40.93 – 45.37 kJ/mol, and Ni-MOF: 40.78 – 44.94 kJ/mol.

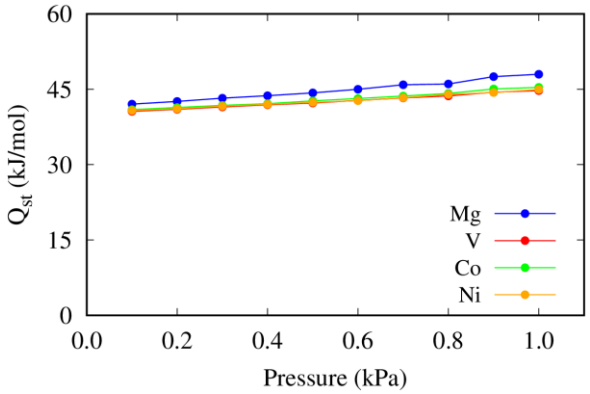

Figure 4. Isosteric heats of SO_2 adsorption for M-MOFs vs the pressure.

The Q_{st} value of SO_2 adsorption is in the order V-MOF ≈ Ni-MOF ≈ Co-MOF < Mg-MOF, exhibiting that SO_2 adsorption on $Mg_2(BDC)_2(TED)$ is the most noticeable as analyzed above.

Moreover, we also research the influence of specific surface area (SSA) and pore volume (V_p) on the adsorptive ability of SO_2 on the M-MOFs. The SSA values are smaller than many other MOFs, but the pore volume is relatively large, as detailed in Table 4. The SSA and pore volume of the M-MOFs are in increasing order Co < Ni < V < Mg. This tendency is consistent with H. Xiang's work for $M(BDC)(TED)_{0.5}$ with M is Ni and Co.[32]

Table 4. The specific surface area and the pore volume of $M_2(BDC)_2(TED)$, compared to another research.

M-MOFs	This work		H. Xiang[32]	
	SSA (m^2/g)	V_p (cm^3/g)	SSA (m^2/g)	V_p (cm^3/g)
M = Mg	1930.95	0.87	-	-
M = V	1727.18	0.78	-	-
M = Co	1627.58	0.74	1708	0.619
M = Ni	1686.09	0.76	1905	0.757

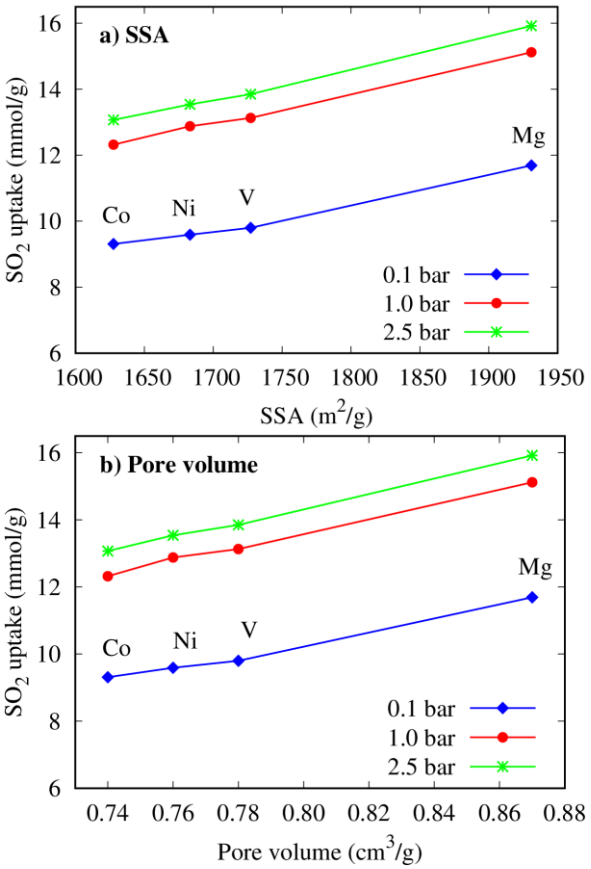

Figure 5. The correlation between the uptakes and (a) the specific surface area (SSA), (b) pore volume (*V*p) of $M_2(BDC)_2(TED)$ at 298 K.

The results in Figure 5 express that the amounts of SO_2 adsorption increase almost entirely linearly with SSA and V_p. Among them, the M-MOF with M = Mg is outstanding, which explains the most excellent SO_2 adsorption into $Mg_2(BDC)_2(TED)$. Therefore, these two structural characteristics (V_p and SSA) have a powerful impact on the ability to capture SO_2 on MOFs at room temperature.

4. CONCLUSION

After optimizing the structure for Ni(BDC)(TED), we replaced the metal to obtain optimized geometries for M(BDC)(TED), with M being Mg, V, and Co by calculations based on vdW-DF. Unit cell volumes are in ascending order of Co < V ≈ Ni < Mg.

The order of metals increasing the SO_2 adsorption uptakes on $M_2(BDC)_2(TED)$ is Co < Ni < V < Mg. At 298K and 2.5 bar, SO_2 uptakes are about 16 mmol/g for Mg-MOF (n_{exc} = 15.82 mmol/g, n_{abs} = 15.92 mmol/g)

and about 13 – 14 mol/g for the M-MOF (M = V, Ni, Co).

Our work also elucidates the factors that enhance the amounts of SO_2 adsorption in $M_2(BDC)_2TED$, including the adsorption isosteric heat, specific surface area, and pore volume. Remarkably, the specific surface areas and pore volumes of M-MOFs almost linearly enhance the SO_2 capture at room temperature and low pressure.

REFERENCES

1. C. Janiak. Metal-organic frameworks with potential application for SO_2 separation and fluegas desulfurization, *ACS Appl. Mater. Interfaces*, **2019**, *11*, 17350−17358.
2. E. Martínez-Ahumada, M. L. Díaz-Ramírez, M. de J. Velásquez-Hernández, V. Jancik and I. A. Ibarra. Capture of toxic gases in MOFs: SO_2, H_2S, NH_3 and NO_x, *Chem. Sci.*, **2021**, *12*, 6772–6799.
3. C. G. Livas, D. Raptis, E. Tylianakis and G. E. Froudakis. Multiscale theoretical study of sulfur dioxide (SO2) adsorption in metal-organic frameworks, *Molecules*, **2023**, *28*, 3122 (1–12).
4. T. T. T. Huong, P. N. Thanh, N. T. X. Huynh and D. N. Son. Metal – organic frameworks: State-of-the-art material for gas capture and storage, *VNU J. Sci. Math. – Phys.*, **2016**, *32*, 67–85.
5. E. Martínez-Ahumada, A. López-Olvera, V. Jancik, J. E. Sánchez-Bautista, E. González-Zamora, V. Martis, D. R. Williams and I. A. Ibarra. MOF materials for thecapture of highly toxic H2S and SO2, *Organometallics*, **2020**, *39*, 883–915.
6. Y. Fu, Z. Wang, S. Li, X. He, C. Pan, J. Yan and G. Yu. Functionalized covalent triazine frameworks for effective CO_2 and SO_2 removal, *ACS Appl. Mater. Interfaces*, **2018**, *10*, 36002–36009.
7. K. Tan, P. Canepa, Q. Gong, J. Liu, D. H. Johnson, A. Dyevoich, P. K. Thallapally, T. Thonhauser, J. Li and Y. J. Chabal. Mechanism of preferential adsorption of SO_2 into two microporous paddle wheel frameworks M(bdc)(ted)0.5, *Chem. Mater.*, **2013**, *25*, 4653–4662.
8. G. Kresse and J. Furthmüller. Efficient iterative schemes for ab initio total-energy calculations using a plane-wave basis set, *Phys. Rev. B*, **1996**, *54*, 11169–11186.
9. G. Kresse and J. Furthmüller. Efficiency of ab-initio total energy calculations for metals and semiconductors using a plane-wave basis set, *Comput. Mater. Sci.*, **1996**, *6*, 15–50.
10. J. P. Perdew, J. Chevary, S. Vosko, K. Jackson, M. Pederson, D. Singh and C. Fiolhais. Atoms, molecules, solids, and surfaces: Applications of the generalized gradient approximation for exchange and correlation, *Phys. Rev. B*, **1992**, *46*, 6671–6687.
11. J. P. Perdew, K. Burke and M. Ernzerhof. Generalized gradient approximation made simple, *Phys. Rev. Lett.*, **1996**, *77*, 3865–3868.
12. P. E. Blöchl. Projector augmented-wave method, *Phys. Rev. B*, **1994**, *50*, 17953–17979.
13. G. Kresse and D. Joubert. From ultrasoft pseudopotentials to the projector augmented-wave method, *Phys. Rev. B*, **1999**, *59*, 1758–1775.
14. J. D. Pack and H. J. Monkhorst. Special points for Brillouin-zone integrations, *Phys. Rev. B*, **1976**, *13*, 5188–5192.
15. M. Methfessel and A. T. Paxton. High-precision sampling for Brillouin-zone integration in metals, *Phys. Rev. B*, **1989**, *40*, 3616–3621.
16. D. Dubbeldam, S. Calero, D. E. Ellis and R. Q. Snurr. RASPA: molecular simulation software for adsorption and diffusion in flexible nanoporous materials, *Mol. Simul.*, **2016**, *42*, 81–101.
17. N. T. X. Huynh, B. T. Duyen, P. T. Tram, T. T. D. Thanh and N. T. M. Duyen. Research on the capture of flue gases of the metal-organic framework $Ni(BDC)(TED)_{0.5}$ by the classical simulation method, *J. Sci. - Quy Nhon Univ.*, **2021**, *15*, 5–12.
18. N. T. X. Huynh, T. T. Nam and D. N. Son. Evaluation of H_2 and CO_2 adsorption into MIL-88A-Fe by Grand canonical Monte Carlo simulation, *J. Sci. - Quy Nhon Univ.*, **2021**, *15*, 5–12.
19. T. A. Manz and N. G. Limas. Introducing DDEC6 atomic population analysis: Part 1. Charge partitioning theory and methodology, *RSC Adv.*, **2016**, *6*, 47771–47801.
20. N. G. Limas and T. A. Manz. Introducing DDEC6 atomic population analysis: Part 2. Computed results for a wide range of periodic and nonperiodic materials, *RSC Adv.*, **2016**, *6*, 45727–45747.
21. T. A. Manz. Introducing DDEC6 atomic population analysis: Part 3. Comprehensive method to compute bond orders, *RSC Adv.*, **2017**, *7*, 45552–45581.
22. N. G. Limas and T. A. Manz. Introducing DDEC6 atomic population analysis: Part 4. Efficient parallel computation of net atomic charges, atomic spin moments, bond orders,

and more, *RSC Adv.*, **2018**, *8*, 2678–2707.
23. H. A. Lorentz. Ueber die anwendung des satzes vom virial in der kinetischen theorie der gase, *Ann. Phys.*, **1881**, *248*, 127–136.
24. D. Berthelot. Sur le mélange des gaz, *Acad. Sci.*, **1898**, *126*, 1703–1855.
25. D. Dubbeldam, K. S. Walton, T. J. H. Vlugt and S. Calero. Design,parameterization, and implementation of stomic force fields for adsorption in nanoporous materials, *Adv. Theory Simulations*, **2019**, *2*, 1900135 (2–62).
26. I. Matito-Martos, A. Martin-Calvo, J. J. Gutiérrez-Sevillano, M. Haranczyk, M. Doblare, J. B. Parra, C. O. Ania and S. Calero. Zeolite screening for the separation of gas mixtures containing SO_2, CO_2 and CO, *Phys. Chem. Chem. Phys.*, **2014**, *16*, 19884–19893.
27. K. Tan, P. Canepa, Q. Gong, J. Liu, D. H. Johnson, P. K. Thallapally, T. Thonhauser, J. Li and Y. J. Chabal. Mechanism of preferential adsorption of SO_2 into two microporous paddle wheel frameworks M(bdc)(ted)0.5, *Chem. Mater.*, **2013**, *25*, 4653–4662.
28. K. Tan, N. Nijem, P. Canepa, Q. Gong, J. Li, T. Thonhauser and Y. J. Chabal. Stability and hydrolyzation of metal organic frameworks with paddle-wheel SBUs upon hydration, *Chem. Mater.*, **2012**, *24*, 3153–3167.
29. M.-A. Eva, D. won Kim, W. Mohammad, C.-M. Paulina, A. López-Olvera, D. R. Williams, V. Martis, H. A. Lara-García, S. López-Morales, D. Solis-Ibarra, G. Maurin, A. I. Ilich and C. S. Hong. Capture and detection of SO_2 by a chemically stable Mg(II)-MOF, *J. Mater. Chem. A*, **2022**, *10*, 18636–18643.
30. V. B. López-Cervantes, D. W. Kim, J. L. Obeso, E. Martínez-Ahumada, Y. A. Amador-Sánchez, E. Sánchez-González, C. Leyva, C. S. Hong, I. A. Ibarra and D. Solis-Ibarra. Detection of SO2 using a chemically stable Ni(II)-MOF, *Nanoscale*, **2023**, *15*, 12471–12475.
31. I. E. Men'shchikov, A. V. Shkolin, E. M. Strizhenov, E. V. Khozina, S. S. Chugaev, A. A. Shiryaev, A. A. Fomkin and A. A. Zherdev. Thermodynamic behaviors of adsorbed methane storage systems based on nanoporous carbon adsorbents prepared from coconut shells, *Nanomaterials*, **2020**, *10*, 1–26.
32. H. Xiang, A. Ameen, P. Gorgojo, F. R. Siperstein, S. M. Holmes and X. Fan. Selective adsorption of ethane over ethylene on M(bdc)(ted)0.5 (M = Co, Cu, Ni, Zn) metal-organic frameworks (MOFs), *Microporous Mesoporous Mater.*, **2020**, *292*, 109724.